Journal of Hazardous Materials 181 (2010) 543–555

Contents lists available at ScienceDirect

Journal of Hazardous Materials

journal homepage: www.elsevier.com/locate/jhazmat

Investigation of 4-year-old stabilised/solidified and accelerated carbonated contaminated soil

A. Antemir[a,*], C.D. Hills[a], P.J. Carey[a], M-C. Magnié[b], A. Polettini[c]

[a] University of Greenwich, Centre for Contaminated Land Remediation, Chatham Maritime ME4 4TB, United Kingdom
[b] INERTEC, 6 rue de Watford, 92000 Nanterre, France
[c] University of Rome "La Sapienza", Department of Hydraulics, Transportation and Roads, Rome, Italy

ARTICLE INFO

Article history:
Received 21 January 2010
Received in revised form 1 May 2010
Accepted 11 May 2010
Available online 16 May 2010

Keywords:
Stabilisation/solidification
Accelerated carbonation
Contaminated soil
Microstructure
Mineralogy
Metal leaching

ABSTRACT

The investigation of the pilot-scale application of two different stabilisation/solidification (S/S) techniques was carried out at a former fireworks and low explosives manufacturing site in SE England. Cores and granular samples were recovered from uncovered accelerated carbonated (ACT) and cement-treated soils (S/S) after 4 years to evaluate field-performance with time. Samples were prepared for microstructural examination and leaching testing. The results indicated that the cement-treated soil was progressively carbonated over time, whereas the mineralogy of the carbonated soil remained essentially unchanged. Distinct microstructures were developed in the two soils. Although Pb, Zn and Cu leached less from the carbonated soil, these metals were adequately immobilised by both treatments. Geochemical modeling of pH-dependent leaching data suggested that the retention of trace metals resulted from different immobilisation mechanisms operating in the two soils examined.

1. Introduction

Approximately 1.2% of the total land surface in the UK is contaminated and poses a threat to human health and the environment [1]. Traditionally, contaminated soils have been landfilled, but as void space declines and costs soar, alternative techniques for soil remediation are being adopted. These include containment (physical, encapsulation or vitrification) and in situ (soil flushing, phytoremediation) and ex situ (physical separation, soil washing, thermal treatments, electrokinetics) extraction techniques [2,3].

Stabilisation/solidification (S/S) and accelerated carbonation (ACT) are containment methods used for the remediation of metal contaminated soil, which allow soil re-development. Stabilisation/solidification decreases the bioavailability/mobility of contaminants in soils, by isolating the contaminants within an impervious mass at a pH at which many contaminants are practically insoluble [4].

Accelerated carbonation (ACT) incorporates another step into S/S. This consists of introducing carbon dioxide (CO_2) during the soil mixing with the cementitious binder, which induces activation of poorly hydraulic cementitious compounds, high early strength and a reduction of pH [5].

The treatment by S/S or ACT does not eliminate the contamination, and therefore the long-term durability and performance of the soils is critical [6,7]. Although ACT has been extensively studied, for the treatment of industrial hazardous wastes [8,9,10,11], it has had limited use for contaminated soil treatment [12]. No full scale treatments have been carried out using ACT, although several pilot-scale trials and laboratory investigations were conducted [13,14]. However, limited data exist on the behaviour of ACT-treated soils over time. Similarly, despite the widespread use of S/S, there is still a lack of field-data pertaining to commercially treated soils [6,7,15].

The present work discusses the findings of a study into a pilot-scale remedial application of accelerated carbonation and traditional cement-based S/S on the same site after 4 years of exposure in the field. The stability of the S/S treated soil and the efficacy of the metal immobilisation by the two treatments is evaluated.

2. Materials and methods

2.1. Site description

The former 8.5 ha Astra Fireworks site in the SE England was used until the early 1990s for the manufacture of low-grade

* Corresponding author at: School of Science, University of Greenwich, Central Avenue, Chatham Maritime ME4 4TB, United Kingdom. Tel.: +44 2083319800; fax: +44 2083319805.
E-mail address: a.antemir@gre.ac.uk (A. Antemir).

0304-3894/$ – see front matter © 2010 Elsevier B.V. All rights reserved.
doi:10.1016/j.jhazmat.2010.05.048

Fig. 1. Soil screening (left) and backfilling in the specially designed cells (right) at the Astra site.

military explosives and fireworks. A hotspot of metals contamination, containing up to 96 000 mg/kg copper, 81 000 mg/kg zinc and 750 mg/kg lead was pilot-treated by excavating, homogenizing and shredding the soil prior to mixing it with cement [16]. A dosage of 20% (w/w) EnvirOceM^{TM}, a superfine sulphate-resisting Portland cement, was added to the excavated soil at a 0.2–0.3 w/c ratio. Three cells of 5 m × 10 m were dug and lined with a high density polyethylene (HDPE) membrane (Fig. 1). One was filled with untreated soil, the second with soil treated with EnvirOceM, further referred as the S/S soil. The third cell contained soil mixed with EnvirOceM, which was dynamically carbonated in a closed chamber for 20 min. The maximum depth of soil in the cells was 0.6 m. Soils were left uncompacted and uncovered to allow the effects of weathering (and rain infiltration) to be maximised.

2.2. Sampling

Core samples of 100 mm diameter were obtained from the untreated, S/S and ACT soils, using a hand driven core cutter, 4 years after treatment. No cores could be recovered from the untreated soil due to the lack of strength and instead granular material was obtained.

The granular samples were quartered, dried and crushed and were used for bulk mineralogy (XRD), chemical characterisation (XRF), pH and metal leaching, as described in Sections 2.2, 2.3 and 2.5. Fragments of core were prepared for microstructural investigation according to the method indicated in Section 2.4.

2.3. X-ray diffraction

Bulk X-ray analyses were performed on powder samples (Siemens D500 X-ray Diffractometer) with a Cu Kα radiation, between 5 and 65° 2θ, a step size of 0.02° and step time of 1.2 s. Clay tiles were prepared for the identification of the clay minerals, according to the method described in Moore and Reynolds [17]. The analysis of the clay was performed using the same instrument and the scanned angles were 2–30° 2θ, step size 0.02° and step time 2.4 s.

2.4. X-ray fluorescence and acid digestion

Bulk chemical analyses of the cement-stabilised soils were carried by the Materials and Engineering Research Institute, Sheffield Hallam University. The oxide composition (major elements) was determined on glass beads, prepared by fusion with lithium tetraborate, using a Philips PW2440 Wavelength Dispersive Spectrometer.The total concentration of minor elements was determined by acid digestion according to the USEPA 3050B method.

2.5. Leaching and geochemical modeling

Granular samples obtained from the untreated, S/S and ACT soil were leached using the TCLP 1311 [18], DIN 38141-S4 [19] and pH-dependent leaching tests, prCEN/TS 15364 [20]. The conditions and key parameters of each leaching test are summarized in Table 1.

The eluates were analysed for major and trace contaminants by ICP-OES (VARIAN Vista MPX) and ion chromatography (Dionex). The pH-dependent leaching data was processed using Visual MINTEQ to predict the equilibrium leachate compositions. The default database was augmented by the solubility constants of minerals available from the literature [21–26], which are listed in Table 2 with reference to the corresponding dissolution reaction. In some cases it was required to rearrange the dissolution reaction to fit with the type of components used by Visual MINTEQ and recalculate the stability constant accordingly. The application of the geochemical speciation code initially involved using the measured concentrations and pH values as input data while suppressing precipitation for all solid phases. Potential solubility-controlling minerals were then chosen in a second step from those displaying saturation indices (SI) in the range $-1.5 \leq SI \leq +1.5$ and on their potential for incorporation in soils and in S/S materials. The predicted equilibrium concentration of each element/species in solution was then calculated using the following equation:

$$C_{pred,i} = C_{meas,i}(10^{-SI_j})^{1/n_{i,j}}$$

where $C_{pred,i}$ and $C_{meas,i}$ are the theoretical and measured concentrations of the ith element/species in solution, SI_j is the saturation index for the jth mineral, and $n_{i,j}$ is the molar coefficient of the ith element/species in the jth mineral.

2.6. Scanning electron microscopy

The specimens were prepared from intact cores recovered from the S/S soils. Fragments of core with dimensions of approximately 30 mm × 30 mm were cast into epoxy resin (Epoxy 301 by Struers).

Table 1
Parameters used in the leaching tests.

	TCLP 1311	DIN 38414-S4	prCEN/TS 15364
Grain size	<10 mm	<9.5 mm	<1mm
L/S ratio	20:1	10:1	10:1
Leachant	Fluid 1 Sodium acetate pH = 4.93 ± 0.05 Fluid 2 Acetic acid pH = 2.88 ± 0.05	Deionised water	HNO_3·0.5M
Leachant renewal	0	0	0
Contact time	18 h	24 h	48 h
Rotation speed	30 rpm	NA	30 rpm

Table 2
Stability constants of the new mineral phases added to the standard thermodynamic database in Visual MINTEQ, based on the dissolution reactions reported.

Mineral	Dissolution reaction	log K	Ref.
Sulphate minerals			
K_2SO_4	$K_2SO_4 \rightarrow 2K^+ + SO_4$	−1.87	[26]
Pentasalt	$(CaSO_4)_5{\cdot}K_2SO_4{\cdot}H_2O \rightarrow 5Ca^{2+} + 2K^+ + 6SO_4 + 6H_2O$	−29.3	[26]
$PbSO_4{\cdot}PbO$	$PbSO_4{\cdot}PbO + 2H^+ \rightarrow 2Pb^{2+} + SO_4 + H_2O$	−0.19	[24]
Syngenite	$K_2Ca(SO_4)_2 \rightarrow Ca^{2+} + 2K^+ + 2SO_4$	−7.45	[26]
C–S–H phases			
Afwillite	$3CaO{\cdot}SiO_2{\cdot}3H_2O + 6H^+ \rightarrow 3Ca^{2+} + 2H_4SiO_4 + 2H_2O$	46.90	[26]
C–S–H(0.8)	$0.8CaO{\cdot}SiO_2{\cdot}2.2H_2O + 1.6H^+ \rightarrow 0.8Ca^{2+} + H_4SiO_4 + H_2O$	11.08	[26]
C–S–H(1.1)	$1.1CaO{\cdot}SiO_2{\cdot}3.9H_2O + 2.2H^+ \rightarrow 1.1Ca^{2+} + H_4SiO_4 + 3H_2O$	16.72	[26]
C–S–H(1.8)	$1.8CaO{\cdot}SiO_2{\cdot}5.2H_2O + 3.6\ H^+ \rightarrow 1.8Ca^{2+} + H_4SiO_4 + 5H_2O$	32.60	[26]
Jennite	$[Ca(OH)_2]_{1.5}{\cdot}(SiO_2)_{0.9}{\cdot}0.9H_2O + 3H^+ \rightarrow 1.5Ca^{2+} + 0.9H_4SiO_4 + 2.1H_2O + 0.485Mg^{2+}$	26.40	[22]
Tobermorite	$[Ca(OH)_2]_2{\cdot}(SiO_2)_{2.4}{\cdot}2H_2O + 4H^+ \rightarrow 2Ca^{2+} + 2.4H_4SiO_4 + 1.2H_2O$	27.81	[22]
AFm phases			
C_4AH_{13}	$2CaO{\cdot}Al_2O_3{\cdot}13H_2O + 14H^+ \rightarrow 4Ca^{2+} + 2Al^{3+} + 20H_2O$	104.42	[22]
C_4FH_{13}	$2CaO{\cdot}Fe_2O_3{\cdot}13H_2O + 14H^+ \rightarrow 4Ca^{2+} + 2Fe^{3+} + 20H_2O$	99.50	[22]
C_2AH_8	$2CaO{\cdot}Al_2O_3{\cdot}8H_2O + 10\ H^+ \rightarrow 2\ Ca^{2+} + 2Al^{3+} + 13H_2O$	60.43	[22]
C_2FH_8	$2CaO{\cdot}Fe_2O_3{\cdot}8H_2O + 10H^+ \rightarrow 2Ca^{2+} + 2Fe^{3+} + 13H_2O$	55.51	[22]
C_2ASH_8	$2CaO{\cdot}Al_2O_3{\cdot}SiO_2{\cdot}8H_2O + 10H^+ \rightarrow 2Ca^{2+} + 2Al^{3+} + H_4SiO_4 + 11H_2O$	49.35	[22]
C_2FSH_8	$2CaO{\cdot}Fe_2O_3{\cdot}SiO_2{\cdot}8H_2O + 10H^+ \rightarrow 2Ca^{2+} + 2Fe^{3+} + H_4SiO_4 + 11H_2O$	44.44	[22]
$C_4AS^*H_{12}$	$3CaO{\cdot}Al_2O_3{\cdot}(CaSO_4){\cdot}12H_2O + 12H^+ \rightarrow 4Ca^{2+} + SO_4^{2-} + 2Al^{3+} + 18H_2O$	74.29	[22]
Cr-monosulphate	$3CaO{\cdot}Al_2O_3{\cdot}(CaSO_4){\cdot}15H_2O + 12H^+ \rightarrow 4Ca^{2+} + CrO_4^{2-} + 2Al^{3+} + 21H_2O$	71.62	[25]
$C_4FS^*H_{12}$	$3CaO{\cdot}Fe_2O_3{\cdot}(CaSO_4){\cdot}12H_2O + 12H^+ \rightarrow 4Ca^{2+} + SO_4^{2-} + 2Fe^{3+} + 18H_2O$	69.37	[22]
$C_4AC^*H_{11}$	$3CaO{\cdot}Al_2O_3{\cdot}(CaCO_3){\cdot}11H_2O + 12H^+ \rightarrow 4Ca^{2+} + CO_3^{2-} + 2Al^{3+} + 17H_2O$	70.52	[22]
$C_4FC^*H_{11}$	$3CaO{\cdot}Fe_2O_3{\cdot}(CaCO_3){\cdot}11H_2O + 12H^+ \rightarrow 4Ca^{2+} + CO_3^{2-} + 2Fe^{3+} + 17H_2O$	65.60	[22]
$C_4AC^*_{0.5}H_{12}$	$3CaO{\cdot}Al_2O_3{\cdot}[Ca(OH)_2]_{0.5}{\cdot}(CaCO_3)_{0.5}{\cdot}11.5H_2O + 13H^+ \rightarrow 4Ca^{2+} + 0.5CO_3^{2-} + 2Al^{3+} + 18.5H_2O$	86.23	[22]
$C_4FC^*_{0.5}H_{12}$	$3CaO{\cdot}Fe_2O_3{\cdot}[Ca(OH)_2]_{0.5}{\cdot}(CaCO_3)_{0.5}{\cdot}11.5H_2O + 13H^+ \rightarrow 4Ca^{2+} + 0.5CO_3^{2-} + 2Fe^{3+} + 18.5H_2O$	85.63	[22]
Fiedel's salt	$3CaO{\cdot}Al_2O_3{\cdot}(CaCl_2){\cdot}10H_2O + 12H^+ \rightarrow 4Ca^{2+} + 2Al^{3+} + 2Cl^- + 16H_2O$	72.04	[26]
Kuzel's salt	$3CaO{\cdot}Al_2O_3{\cdot}(CaCl_2)_{0.5}(CaSO4)_{0.5}{\cdot}12H_2O + 12H^+ \rightarrow 4Ca^{2+} + 2Al^{3+} + Cl^- + 0.5SO_4^{2-} + 18H_2O$	71.94	[26]
AFt phases			
Cl-ettringite	$Ca_6Al_2Cl_6(OH)_{12}{\cdot}24H_2O + 12H^+ \rightarrow 6Ca^{2+} + 2Al^{3+} + 6Cl^- + 36H_2O$	56.84	[26]
Cr-ettringite	$Ca_6Al_2(CrO_4)_3(OH)_{12}{\cdot}26H_2O + 12H^+ \rightarrow 6Ca^{2+} + 2Al^{3+} + 3CrO_4^{2-} + 38H_2O$	60.54	[25]
Fe-ettringite	$Ca_6Fe_2(SO_4)_3(OH)_{12}{\cdot}26H_2O + 12H^+ \rightarrow 6Ca^{2+} + 2Fe^{3+} + 3SO_4^{2-} + 38H_2O$	51.98	[22]
Tricarboaluminate	$Ca_6Al_2(CO_3)_3(OH)_{12}{\cdot}26H_2O + 12H^+ \rightarrow 6Ca^{2+} + 2Al^{3+} + 3CO_3^{2-} + 38H_2O$	60.69	[22]
(Hydro)garnets			
C_3AS_3	$3CaO{\cdot}Al_2O_3{\cdot}(SiO_2)_3 + 12H^+ \rightarrow 3Ca^{2+} + 2Al^{3+} + 3H_4SiO_4$	52.55	[26]
C_3AH_6	$3CaO{\cdot}Al_2O_3{\cdot}6H_2O + 12H^+ \rightarrow 3Ca^{2+} + 2Al^{3+} + 12H_2O$	79.528	[22]
$C_3AS_{0.5}$	$3CaO{\cdot}Al_2O_3{\cdot}(SiO_2)_{0.5}{\cdot}5H_2O + 12H^+ \rightarrow 3Ca^{2+} + 2Al^{3+} + 0.5H_4SiO_4 + 10H_2O$	74.12	[26]
C_3ASH_4	$3CaO{\cdot}Al_2O_3{\cdot}SiO_2{\cdot}4H_2O + 12H^+ \rightarrow 3Ca^{2+} + 2Al^{3+} + H_4SiO_4 + 8H_2O$	69.37	[26]
C_3FH_6	$3CaO{\cdot}Fe_2O_3{\cdot}6H_2O + 12H^+ \rightarrow 3Ca^{2+} + 2Fe^{3+} + 12H_2O$	74.61	[22]
CAH_{10}			
CAH_{10}	$CaO{\cdot}Al_2O_3{\cdot}10H_2O + 8H^+ \rightarrow Ca^{2+} + Al^{3+} + 14H_2O$	38.51	[22]
Mg phases			
Hydrotalcite	$Mg_4Al_2(OH)_{14}{\cdot}3H_2O + 14H^+ \rightarrow 2Al^{3+} + 4Mg^{2+} + 17H_2O$	73.96	[22]
CO_3-hydrotalcite	$Mg_4Al_2(OH)_{12}{\cdot}CO_3{\cdot}2H_2O + 12H^+ \rightarrow 4Mg^{2+} + CO_3^{2-} + 2Al^{3+}$	50.85	[22]
Other phases			
Akermanite	$Ca_2MgSi_2O_7 + 6H^+ + H_2O \rightarrow 2Ca^{2+} + Mg^{2+} + 2H_4SiO_4$	46.08	[23]
Anorthite	$CaO{\cdot}Al_2O_3{\cdot}(SiO_2)_2 + 8H^+ \rightarrow Ca^{2+} + 2Al^{3+} + 2H_4SiO_4$	25.31	[23]
C_3A	$3CaO{\cdot}Al_2O_3 + 12H^+ \rightarrow 2Al^{3+} + 3Ca^{2+} + 6H_2O$	113.05	[26]
C_4AF	$4CaO{\cdot}Al_2O_3{\cdot}Fe_2O_3 + 20H^+ \rightarrow 2Al^{3+} + 2Fe^{3+} + 4Ca^{2+} + 10H_2O$	140.51	[26]
Ca oxychloride	$3CaO{\cdot}CaCl_2{\cdot}16H_2O + 6H^+ \rightarrow 4Ca^{2+} + 2Cl^- + 19H_2O$	68.75	[26]
Ca zincate	$CaZn_2(OH)_6{\cdot}2H_2O + 6H^+ \rightarrow Ca^{2+} + 2Zn^{2+} + 8H_2O$	43.90	[21]
Ca-zeolite P	$CaO{\cdot}Al_2O_3{\cdot}(SiO_2)_{2.6}{\cdot}3.2H_2O + 8\ H^+ \rightarrow Ca^{2+} + 2\ Al^{3+} + 2.6\ H_4SiO_4 + 2\ H_2O$	20.20	[26]
Chabazite	$CaO{\cdot}Al_2O_3{\cdot}(SiO_2)_4{\cdot}6H_2O + 8H^+ \rightarrow Ca^{2+} + 2Al^{3+} + 4H_4SiO_4 + 2H_2O$	13.63	[26]
Forsterite	$Mg_2SiO_4 + 4H^+ \rightarrow 2Mg^{2+} + H_4SiO_4$	28.60	[23]
Gehlenite	$2CaO{\cdot}Al_2O_3{\cdot}SiO_2 + 10H^+ \rightarrow 2Ca^{2+} + 2Al^{3+} + H_4SiO_4 + 3H_2O$	55.23	[23]
Leucite	$KAl(SiO_3)_2 + 2H_2O + 4H^+ \rightarrow K^+ + Al^{3+} + 2H_4SiO_4$	6.42	[21]
Merwinite	$Ca_3Mg(SiO_4)_2 + 8H^+ \rightarrow 3Ca^{2+} + Mg^{2+} + 2H_4SiO_4$	69.28	[23]
Na-zeolite P	$Na_2O{\cdot}Al_2O_3{\cdot}(SiO_2)_{2.6}{\cdot}3.2H_2O + 8H^+ \rightarrow Ca^{2+} + 2Al^{3+} + 2.6H_4SiO_4 + 2H_2O$	26.40	[26]
$ZnFe_2O_4$	$ZnFe_2O_4 + 8H^+ \rightarrow Zn^{2+} + 2Fe^{3+} + 4H_2O$	9.85	[24]
$ZnSiO_3$	$ZnSiO_3 + H_2O + H^+ \rightarrow Zn^{2+} + H_4SiO_4$	2.93	[21]
Wairakite	$CaO{\cdot}Al_2O_3{\cdot}(SiO_2)_4{\cdot}2H_2O + 2H_2O + 8H^+ \rightarrow Ca^{2+} + 2Al^{3+} + 4H_4SiO_4$	18.87	[21]
Wollastonite	$CaSiO_3 + H_2O + H^+ \rightarrow Ca^{2+} + H_4SiO_4$	12.99	[21]

The blocks were ground by hand to expose the surfaces to be analysed, using successive SiC paper with decreasing grit sizes (30, 15 and 10 μm). The resin blocks were polished on an Engis polishing machine, with progressively decreasing grit size diamond pastes (3, 1 and 0.25 μm), supplied by Struers. Between each stages of grinding and polishing, the resin blocks were cleaned in absolute ethanol.

Prior to the SEM analysis the blocks were carbon coated and analysed with an SEM (JEOL JSM 5310-LV) equipped with a LaB_6 filament and Energy Dispersive Spectrometer (EDS). Backscattered electron images (BSE) were collected using a 20 kV accelerating voltage. X-ray microanalysis provided qualitative and semi-quantitative compositional information.

Table 3
Mineral phases identified by XRD in Astra soil at different ages.

Sample	Age (months)	Mineral phases										
		Quartz	Kaolinite	Montmorillonite	Muscovite	Hematite	C_2S	C_3S	Calcite	Aragonite	Portlandite	Ettringite	Bassanite	Pyrite
Untreated	0[a]	•	•	•	•									•
	16[a]	•	•	•	•									•
	48	•	•	•	•									
S/S	0[a]	•	•	•	•		•	•	•	•				
	16[a]	•	•	•	•		•		•					
	48	•	•	•	•	•					•	•	•	
ACT	0[a]	•	•	•	•		•	•	•	•				
	16[a]	•	•	•	•		•		•	•				
	48	•	•	•	•				•					

[a] From [16].

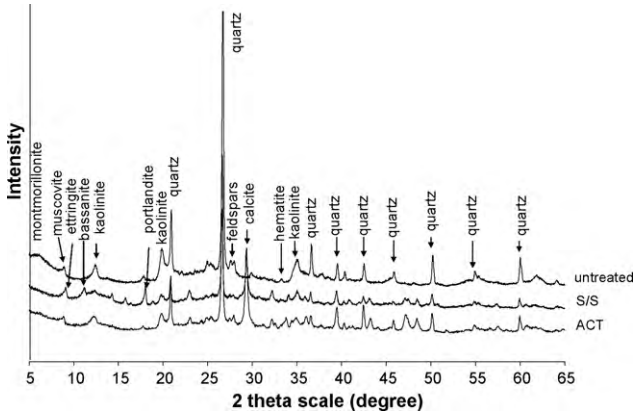

Fig. 2. Diffractograms from the 4-year-old, weathered treated and untreated soils.

3. Results

3.1. Mineralogical composition

Examination of the Astra soil mineralogy was carried out at different ages and the findings are shown in Table 3. The main minerals found in the three soils were quartz (SiO_2), montmorillonite $(Na,Ca)_{0.33}(Al,Mg)_2(Si_4O_{10})(OH)_2{\cdot}nH_2O$), kaolinite ($Al_2Si_2O_5(OH)_4$), muscovite ($KAl_2AlSi_3O_{10}(OH)_2$, hematite ($Fe_2O_3$), pyrite ($FeS_2$) and feldspars. Portlandite ($Ca(OH)_2$), ettringite ($Ca_6Al_2(SO_4)(OH)_{12}{\cdot}26H_2O$), calcite ($CaCO_3$), bassanite ($CaSO_4{\cdot}1/2H_2O$) and anhydrous cement phases such as calcium di/tri silicates (C_2S and C_3S) were observed in the treated soils. Initially, the treated soils contained calcium silicates, soil derived minerals and calcium carbonates, in the case of the ACT soil; however subsequently secondary minerals such as ettringite and bassanite formed in the S/S soil (Fig. 2).

3.2. Microstructure of soils

Representative samples from untreated, S/S and ACT soils were prepared in thin section and analysed by SEM. Prior to the SEM analysis, photographs of the thin section were taken. These show the distinct structures observed in the untreated and treated soils, as shown in Fig. 3.

The resin-impregnated untreated clayey soil is bisected by desiccation cracks (yellow-coloured resin-rich areas) and contains fragments of brick and opaque slag (Fig. 3a). The S/S soil was finer-grained and contained dark brown clay agglomerations, of up to 0.5 cm in size, (Fig. 3b). In contrast to the cement-treated soil, the carbonated soil contained 'pebble-like' formations, consisting of spherical soil agglomerates enveloped in a carbonate coating (Fig. 3c). The microstructure of the two treated soils was found to be distinct (Fig. 4c–f). The less porous S/S soil contained stratified precipitates in pore space which could be seen with the unaided eye. The formation of these was facilitated by periodic wetting and drying episodes over the 4 years of field exposure during time of lower than average rainfall.

Fig. 4c shows a typical clay agglomerate, surrounded by light grey-coloured crustiform calcium carbonate. The circled area (Fig. 4d) shows the calcium carbonate matrix bordered by clay (top right). The ACT soil contained clay coated by carbonated decalcified cement, up to 100 μm thick (Fig. 4e and f). The carbonated rim in Fig. 4f is sandwiched between clay intermixed with quartz and cement grains. An examination of the rim showed persistent anhydrous cement grains co-existing with highly decalcified cement grains, characterised by a Si-rich pseudomorph enveloped in calcium carbonate.

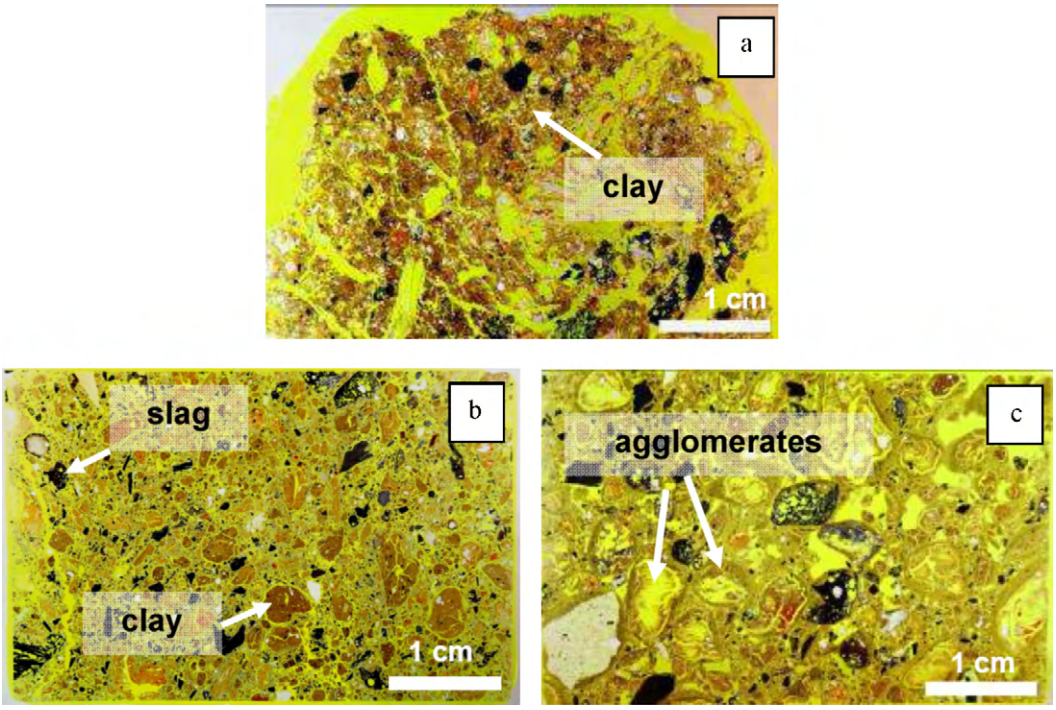

Fig. 3. The thin sections prepared from 4-year-old (a) untreated, (b) S/S and (c) ACT soil.

Ettringite was abundant in the S/S soil. Fig. 5 shows radiating clusters of ettringite infilling void space within the matrix, or intermixed with the outer C–S–H hydration product and portlandite (not shown here).

Metal contaminants were identified in the untreated soil, which were not observable in the S/S and ACT soils, resulting from dilution by cement addition, physical comminution, or by the dissolution/dispersion of particles during initial mixing at high pH.

The contaminants were present as sub-rounded fragments of individual metals of up to 50 μm in size or as grains of mixed metals up to 200 μm dispersed in the clay matrix. Zn was in particular associated with Fe and montmorillonite, as shown in Fig. 6. This clay mineral was identified by XRD and confirmed by the EDS point analysis (spectrum 2).

3.3. Chemical characterisation

The pH of the untreated soil was neutral, whilst that of the ACT and S/S soils was mildly to highly alkaline and equal to 8.9 and 12.3, respectively.

Table 4 presents the oxide composition obtained from the untreated and treated soils. These were composed of SiO_2, Al_2O_3, Fe_2O_3 and CaO, comprising up to 70% of the total weight of sample. The metal contaminants were Cu, Pb, Zn and Cr. As seen from Table 5, the concentration of these heavy metals was generally higher in the untreated than in the treated soils. This difference was ascribed to the dilution effect by the addition of cement binders.

Table 4
Oxide analysis of the 4-year-old Astra soils.

Oxide	Composition (%)		
	Untreated soil	S/S soil	ACT soil
SiO_2	49.7	34.4	41.3
Al_2O_3	14.5	12.5	12.1
Fe_2O_3	6.7	6.4	6.1
Na_2O	0.3	0.3	0.3
CaO	1.4	16.5	12.7
MgO	1.2	1.2	1.2
K_2O	2.0	1.4	1.7
P_2O_5	0.2	0.2	0.1
BaO	0.1	0.1	0.1
SO_3	0.2	0.2	0.7
LOI	22.7	25.9	23.4

3.4. Metal leaching

3.4.1. Regulatory leaching tests

When the remedial trial was conducted at the Astra site, the leaching testing methods across Europe were not yet harmonized and this is reflected in the methods chosen at that time.

Three samples for each type of soil were leach tested immediately after remediation and after 4 years, according to two pass/fail tests (DIN 38414-S4 and TCLP 1311) and the results are presented in Table 6. These show that the leaching from the S/S and ACT soils remained below the set thresholds for all four metals of concern. The untreated soil exceeded the limit for Zn, using the TCLP 1311 leaching test. It should be noted that although historically the S/S treated soils leached Zn and Cu above the set threshold, this decreased with time by more than one order of magnitude.

3.4.2. pH-dependent leaching test and modeling of leaching data

Fig. 7 shows the pH-dependent leaching results for the four metal contaminants of concern (Cr, Cu, Pb and Zn). It was observed that the shape of the leaching curves changed dramatically upon

Table 5
Total contaminant concentration in the 4-year-old Astra soils.

Element	Concentration (mg/kg)		
	Untreated soil	S/S soil	ACT soil
Zinc	1324 ± 144	735 ± 79	696 ± 185
Lead	138 ± 15	85 ± 29	100 ± 13
Chromium	35 ± 7	18 ± 2	26 ± 1
Copper	543 ± 142	228 ± 58	146 ± 27

Errors represent the standard deviation of three replicate samples.

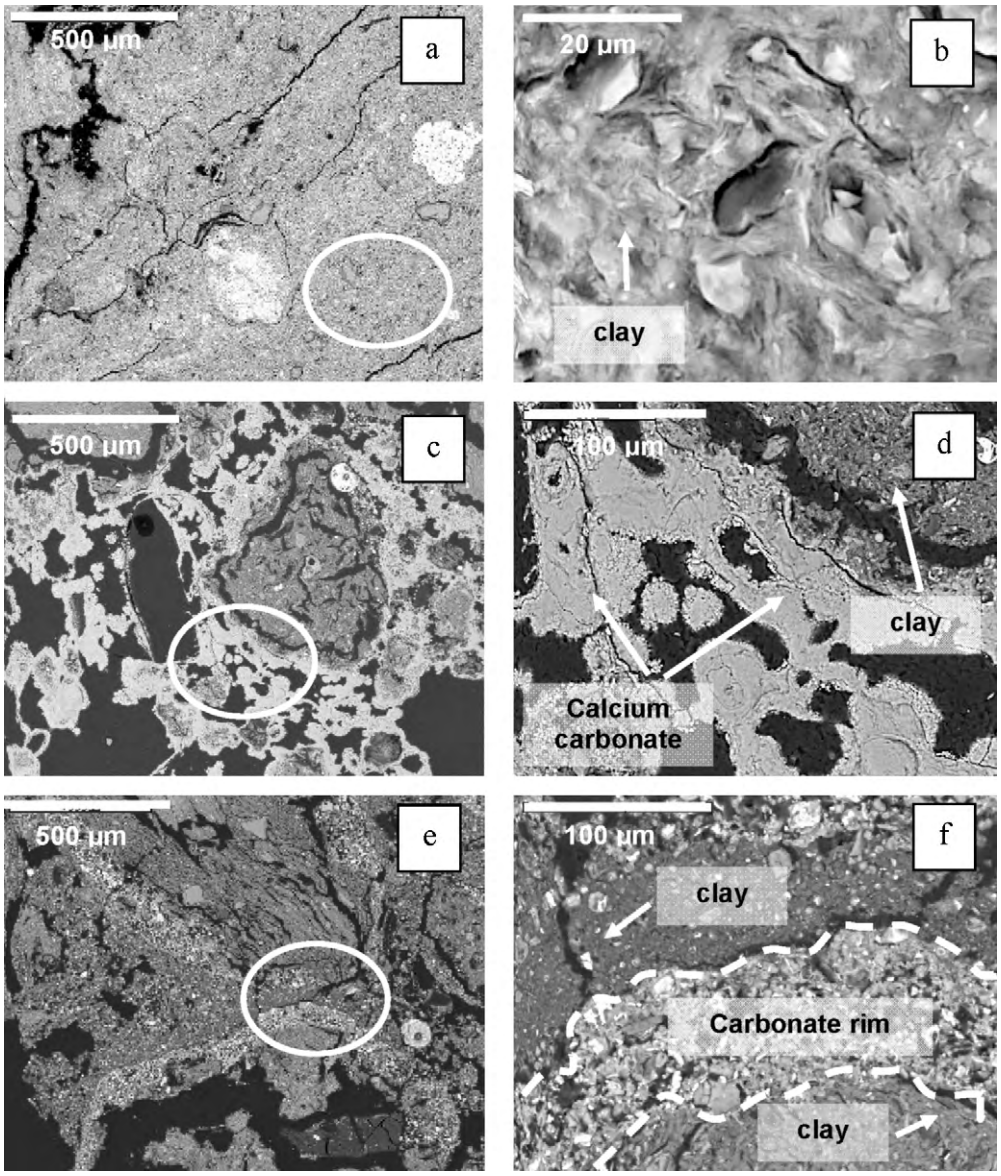

Fig. 4. Backscattered electron micrographs showing clay in the untreated soil (a and b); calcium carbonate infilling voids in the matrix of the S/S soil (c and d); pebble-like formations in the ACT soil and magnification of the circled area (e and f).

Table 6
Metals leached from untreated, S/S and ACT soil after remediation and 4 years later (mg/l).

	Leaching limit	Untreated soil		S/S soil		ACT soil	
		Historical[a]	After 4 years	Historical*	After 4 years	Historical*	After 4 years
DIN							
Zn	5	0.20	1.17 ± 0.26	0.03	0.01	n.d.	0.04 ± 0.02
Pb	0.05	0.02	0.04 ± 0.01	n.d.	n.d.	n.d.	n.d.
Cr	0.1	0.01	n.d.	0.05	0.03	0.03	0.01 ± 0.01
Cu	5	0.05	0.39 ± 0.04	0.94	0.61 ± 0.02	0.04	0.33 ± 0.13
TCLP							
Zn	5	391	9.02 ± 1.64	82	n.d.	3.13	0.35 ± 0.07
Pb	5	0.18	0.14	0.02	n.d.	n.d.	n.d.
Cr	5	n.d.	0.12	0.02	0.01	0.02	0.01
Cu	1	152	0.55 ± 0.02	11	0.9	0.14	0.15 ± 0.01

Errors represent standard deviations of three replicate samples.
n.d. signifies elements not detected.
Note historical data were not reported with associated errors.
[a] [16].

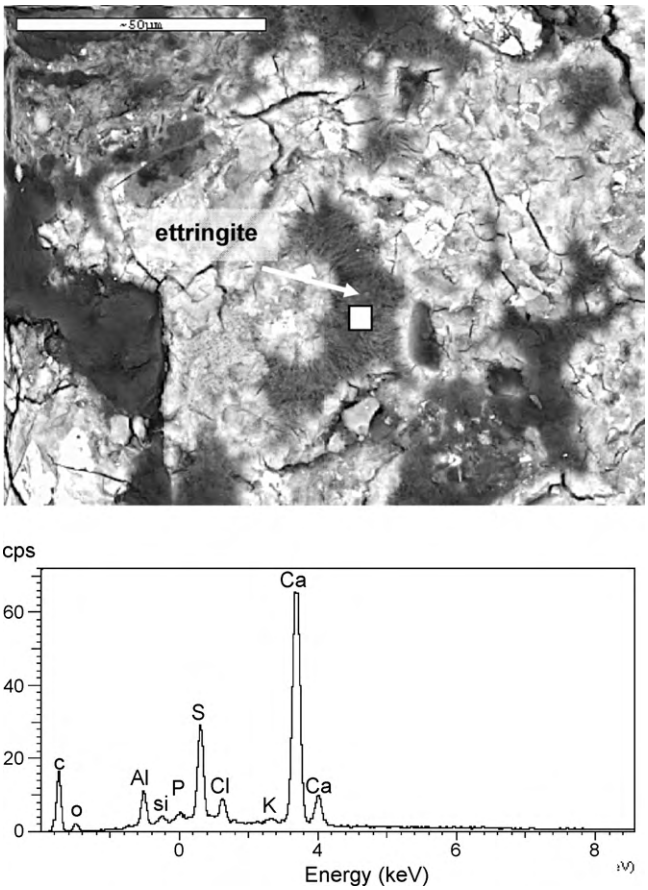

Fig. 5. Backscattered electron micrograph showing radiating clusters of ettringite growing in voids in the S/S soil and the characteristic EDS point analysis of the ettringite taken from the marked area.

treatment, providing a strong indication of different chemical phenomena governing the release of contaminants from the treated material. Differences in the pH-dependent release of heavy metals were also observed between the S/S and the ACT soils, suggesting that the metal immobilisation mechanisms changed when accelerated carbonation was applied to the soil/binder system.

However, irrespective of this heavy metal leaching was reduced by one to two orders of magnitude in comparison to the untreated soil, particularly in the alkaline pH range. However, in the S/S soil, the metal leaching data correlated with the major element concentrations (Ca, Al and Si) in solution (indicating either encapsulation or incorporation in the alumino-silicate hydration phases), whereas for the ACT-treated soil this relationship was much less evident.

The results of the modeling using Visual MINTEQ are reported in Figs. 8–10 for the untreated, S/S and ACT soils, respectively. The measured concentrations in the leachates, as a function of pH, are compared with the predicted solubility curves of candidate solid phases for the solubility control for the element/species of concern. Since it is typical for materials of different nature that the mineral phases which govern the leaching of a given element/species change depending on the pH conditions, different pH domains can be identified on the basis of the most probable candidate phase for solubility control. The overall theoretical solubility curve for a certain element is thus derived as the envelope of the theoretical curves for solubility-controlling minerals in different pH regions, which are plotted individually in Figs. 8–10.

For the untreated soil (see Fig. 8) the most probable solubility-controlling phases for Al included leucite ($KAlSi_2O_6$) at pH values below 7.4 and amorphous $Al(OH)_3$ above this value. Leucite may also control the solubility of Si in the same pH range as for Al. At higher pHs amorphous silica was the best fit with the Si leaching data. Although quartz was identified by XRD (see Fig. 2) no evidence for solubility control by this phase was obtained by modeling the leaching solutions.

For Ca and SO_4, the model predictions described the data well over a limited pH range. In particular, the phases identified for Ca and SO_4 in the pH range 7.4–8.6 were calcite ($CaCO_3$) and barite ($BaSO_4$), respectively. At other pHs, however, modeling indicated that complex solid phases not included in the expanded database were important.

For the metals of concern, leaching as a function of pH was not attributed to any mineral present in the thermodynamic database used for modeling; the only exception was Cu under alkaline conditions, with tenorite (CuO) describing the solubility of this metal at pH > 8. The absence of key phases for trace metals suggests that metal contaminants were present in the soil in complexes that are difficult to describe as pure solids. Such a hypothesis appears to be supported by the findings from microstructural observations, where, for example, Zn was associated with the Al-bearing soil minerals and clay particles.

For the S/S soil (see Fig. 9), Al leaching appeared to be dominated by the hydrous oxides $Al(OH)_3$ or boehmite (AlOOH) at low pH values and possibly by gehlenite hydrate/strätlingite (an AFm phase with the composition: $2CaO{\cdot}Al_2O_3{\cdot}SiO_2{\cdot}8H_2O$). With respect to this phase, however, it should be noted that in the range where gehlenite hydrate was found to fit the experimental data, Al concentrations were in the order of magnitude of the analytical detection limit, and this was taken as the input value for the modeling calculations. It may also be probable that other less soluble phases may have controlled the (trace) level-leaching of Al in solution at pHs > 10.

The alkaline release of Ca and Si from the S/S soil appeared to be controlled by Ca-rich C–S–H phases, including jennite (Ca/Si = 1.7) and C–S–H (Ca/Si = 1.8). In the same pH range, leachates were found to be slightly oversaturated in ettringite. At acidic pH values, the leaching of Ca and Si was dictated by gypsum and leucite, respectively. Although carbonated phases were described in the S/S soil (see above for details), none informed the leaching behaviour of major elements in the treated material.

As a consequence of the effects of accelerated carbonation on the hydration process, the solubility-controlling minerals were predicted to be different from those in the S/S soil. Upon carbonation (Fig. 10), the leaching of Al decreased by approximately two orders of magnitude (and even more in the acidic pH range), so that the very soluble Al hydrous oxide phases could no longer describe the release of this metal. In the acidic pH range, the less soluble hydrous oxide, diaspore (AlOOH), broadly fit the experimental data, but could not explain the overall leaching data obtained for Al. For pH values > 8 either microcline ($KAlSi_3O_8$) or chabazite, ($CaAl_2Si_4O_{12}{\cdot}6H_2O$, a zeolite) were identified as potential solubility-controlling phases for Al and Si.

As the leaching solutions were always found to be strongly (> than one order of magnitude) undersaturated with respect to common cement hydrates, including C–S–H (irrespective of the Ca/Si ratio considered), AFm and AFt phases, other phases must have been important. For Ca for example, in the limited pH range (pH = 5.3–6.7), gypsum and the mono-hydrated Ca carbonate ($CaCO_3{\cdot}H_2O$) also known as monohydrocalcite (at higher pH values) may have been involved. The latter is recognised as being more soluble than its respective unhydrated polymorphs and is preferentially formed in the presence of Mg. As such, some other seawater constituent ions, organic material and microrganisms (see e.g. [27,28]) were involved. It is noteworthy that the Ca^{2+} and CO_3^{2-} ions released by calcite dissolution from the ACT soil during the pH-dependent leaching test and the high con-

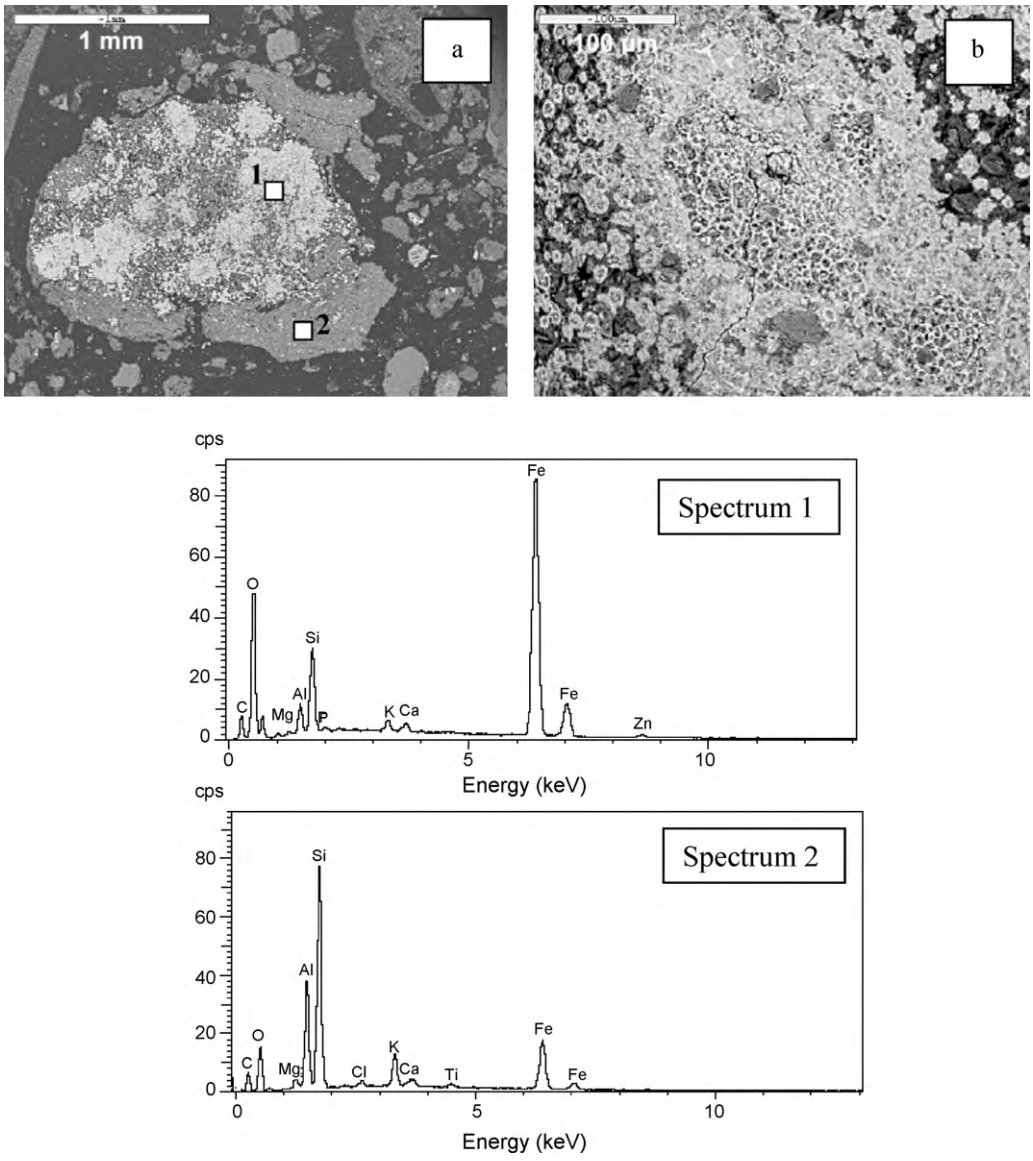

Fig. 6. Backscattered electron micrographs showing contamination of the untreated soil. (a) Soil particle contaminated with Fe and Zn and (b) magnification of the contamination area. EDS spectrum 1 corresponds to the contaminated area containing Fe and Zn and spectrum 2 to the clay soil.

centrations of major cations were favorable to the formation of $CaCO_3 \cdot H_2O$.

As mentioned, the leachate concentrations of Cr, Cu, Pb and Zn were significantly decreased by S/S and ACT. It was also found that the accelerated carbonation treatment was more effective than the conventional S/S process towards trace metal immobilisation. Furthermore, in the treated soils, the heavy metals of concern leached at appreciably lower levels than predicted for their respective oxide, hydroxide and silicate mineral-forms included in the expanded Visual MINTEQ database. In the S/S soil, this may indicate encapsulation or incorporation of these metals in the mineral structure of the hydration phases formed, while no evidence for this was gained from the ACT soil. It is thus hypothesized that the formation of carbonate minerals during ACT treatment may explain the observed metal release. However, only in the case of Zn was some evidence gained of the formation of pure metal carbonates, with smithsonite ($ZnCO_3$) being a possible candidate in the pH range 5.3–8.3, typical of carbonate stability. For the other metals investigated, it may be argued that precipitation of complex carbonate phases or sorption onto the surface of neo-formed minerals may have determined the actual mechanisms of metal immobilisation within the matrix.

3.4.3. Acid neutralisation capacity (ANC)

Fig. 11 describes the variation of pH with acid addition for the untreated, S/S and ACT soils. The untreated soil displayed a low $ANC_{4.0}$ of 0.1 mequiv./g, whilst the treated soils required additions of up to 4.6 meq/g to reduce the pH from the natural value to 4. Although both treated soils showed an improved ANC compared to the untreated soil and had distinct shaped ANC curves. The ANC curve for the S/S soil was characterised by plateau between pH 12 and 10, followed by a steep drop to pH 5 and another plateau at pH 4.

The most significant difference of the ACT soil compared to the S/S soil was the lack of buffering capacity at high pH (>10). This was due to the consumption, during accelerated carbonation, of portlandite, the main phase controlling the equilibrium pH around 12.3 [29]. The ANC curve displayed a steep gradient from pH 6.3 to 8.8 with low acid additions (<0.5 meq/g), followed by a plateau between pH 5 and 6.7 and a steady drop below pH 5. Fig. 11 shows

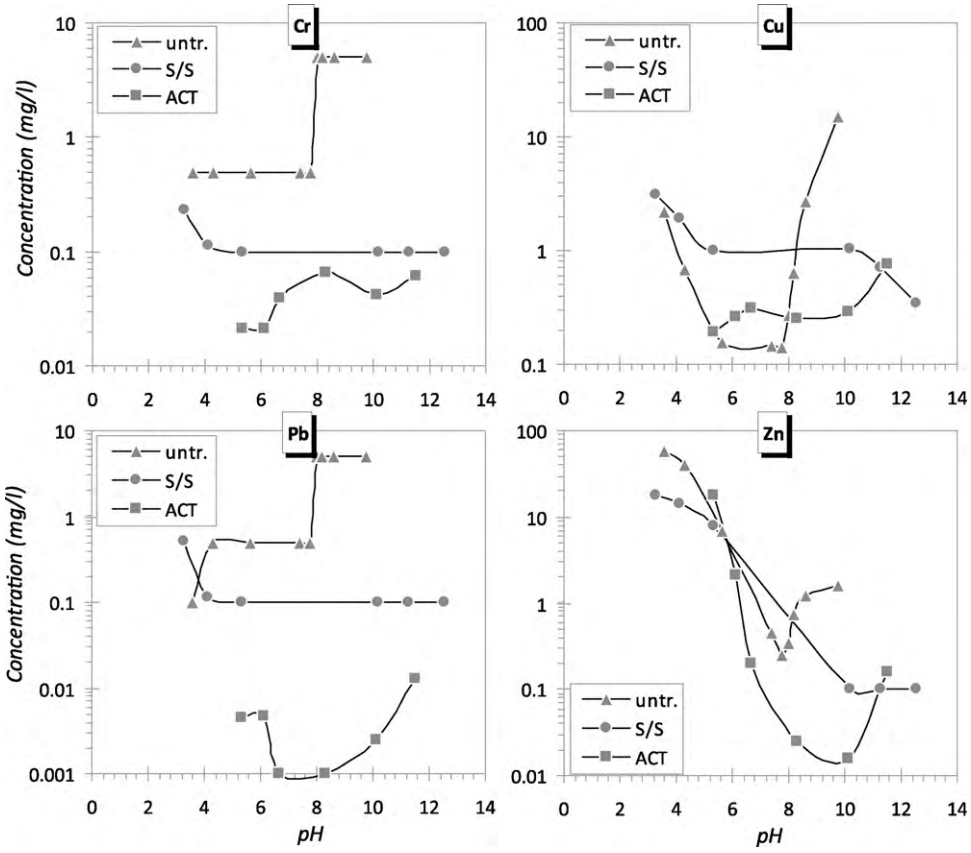

Fig. 7. pH-dependent leaching of Cr, Cu, Pb and Zn for the untreated, S/S and ACT soil.

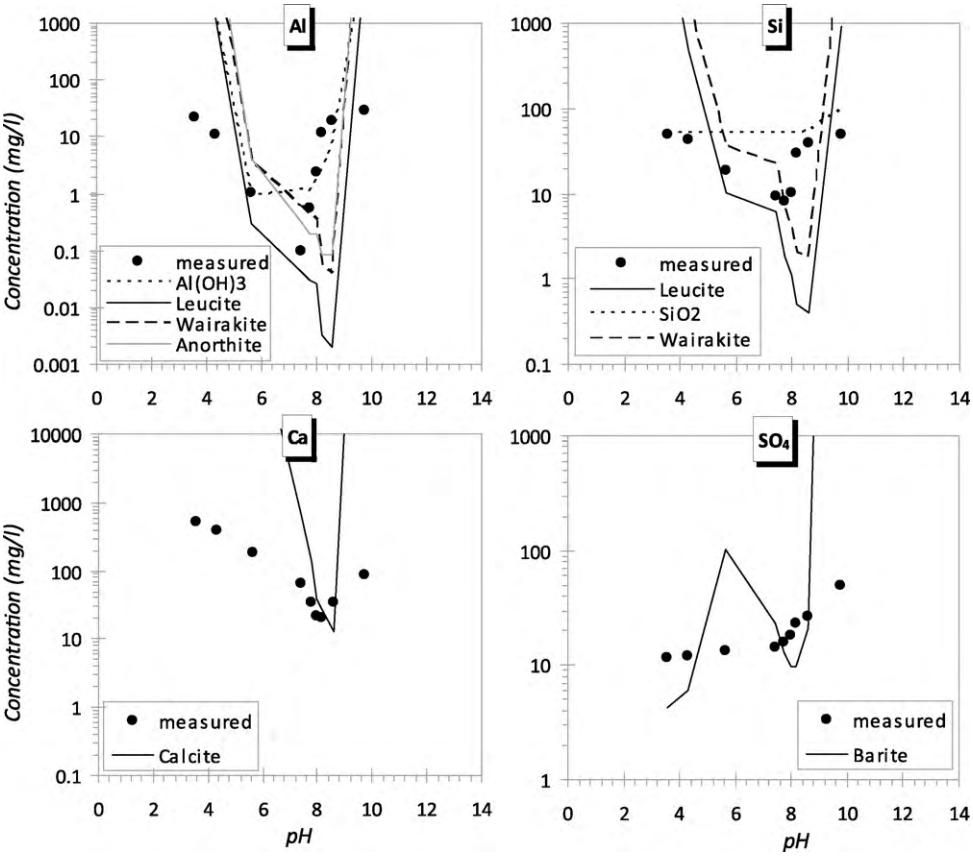

Fig. 8. Experimental data (black dots) and model predictions (continuous lines) for Al, Si, Ca and sulfate leaching from the untreated soil.

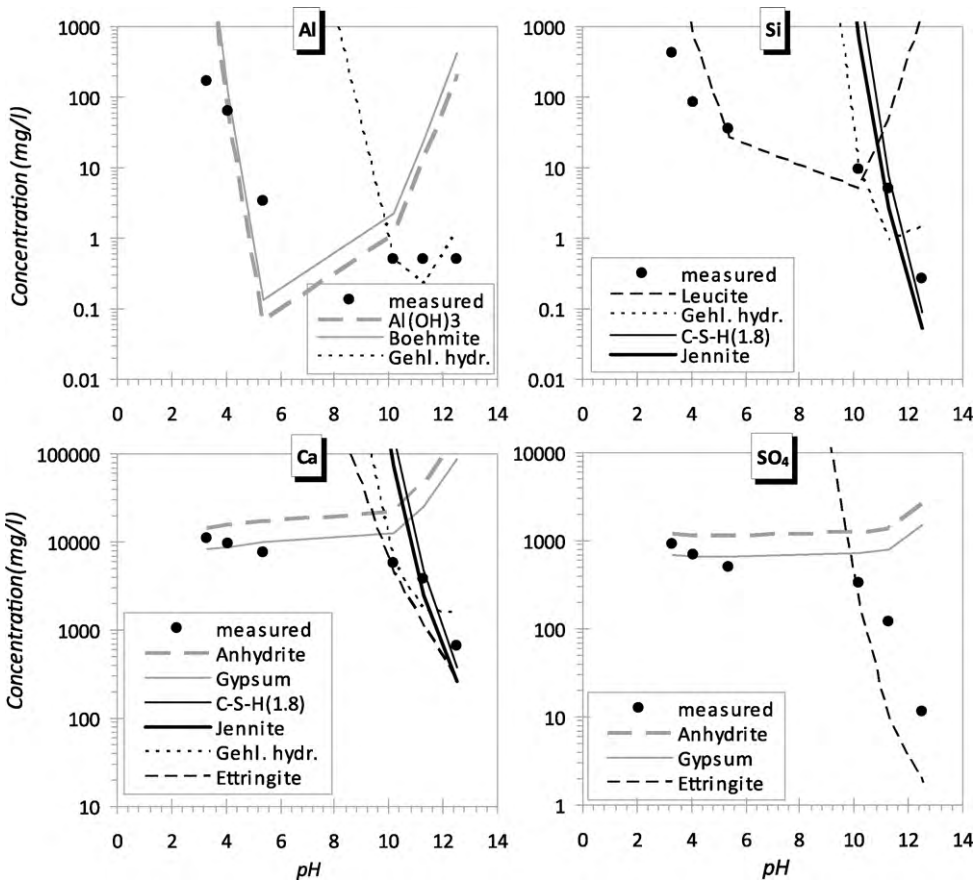

Fig. 9. Experimental data (black dots) and model predictions (continuous lines) for Al, Si, Ca and sulfate leaching from the S/S soil.

that the $ANC_{4.0}$ of the ACT soil was 3.5 meq/g, slightly lower than that of the S/S soil equal to 4.6 meq/g.

4. Discussion

This work has provided an insight into the effect of weathering upon 4-year-old soils treated by stabilisation/solidification and accelerated carbonation. The soils were left uncompacted and exposed to the atmosphere in a 'worse-case' exposure scenario. The data suggest that the two treatments behaved very differently to identical environmental loads over time-scale investigated.

4.1. Microstructure

Mineralogical change was observed in both the treated soils, as indicated in Table 1. At 0 and 16 months the ACT soil contained observable calcium carbonate (calcite and aragonite) and occasional anhydrous cement grains. The S/S soil had a similar mineralogy to the ACT soil at early age, but secondary minerals like ettringite ($Ca_6Al_2(SO4)_3(OH)_{12}\cdot 26H_2O$) formed at about 48 months of age. Despite the extreme exposure environment, portlandite ($Ca(OH)_2$) was observed in the 4-year-old S/S soil.

In the S/S soil, atmospheric carbonation proceeded due to the exposure environment. It is widely accepted that carbonation is deleterious to structural concrete [30], but for S/S systems this is not necessarily the case [10,11].

Massive primary carbonate production formed during accelerated carbonation treatment and this was characterised by the formation of carbonate shells around soil particles, whilst in the S/S soil the secondary carbonation of cement hydration products resulted. The effect of this on the microstructure of the S/S soil was significant. Distinct layers of calcium carbonate (up to 500 μm) were visible in the porosity, indicating intermittent precipitation during wetting and drying cycles. In the same way as in exposed concretes, carbonation of the S/S soils is promoted during drying stages and inhibited by wet stages, when the pores are saturated [12,31]. This carbonate resulted from the reaction of portlandite with atmospheric CO_2.

Another mineral formed in the S/S soil was ettringite. This is common in environmentally exposed concretes [31] and can, in some cases, cause disruption to the hardened structure [32]. Ettringite is closely linked to fluid transport in the soil [33] and was identified in the vicinity of portlandite. Many authors have recognised the benign effect of this type of ettringite which freely deposits in available pore space [31,34,35]. Since the Astra soil was granular rather than monolithic in nature it appears able to accommodate any expansive growth. The presence of bassanite (dehydrated gypsum) in the treated soils may indicate that several mechanisms are active: gypsum may result from the decomposition of ettringite at pH below 10.5 [36], or it can form instead of ettringite when the aluminium is depleted and soluble sulfates are present [37]. Bassanite might also be an artefact of sample preparation [38], and as far as this study is concerned, it is unclear which mechanism leads to gypsum formation in the treated soils. In general, sulfate attack is a term to describe the damage caused by sulfate-bearing phases i.e. ettringite, gypsum, thaumasite, but this does not apply to the Astra soils, since there was no damaging effect associated with their presence.

By comparison with the S/S soil, the structure of the ACT soil remained largely unchanged over the 4 years of weathering. Although two calcium carbonate polymorphs (calcite and aragonite) were identified soon after the treatment with CO_2, only calcite

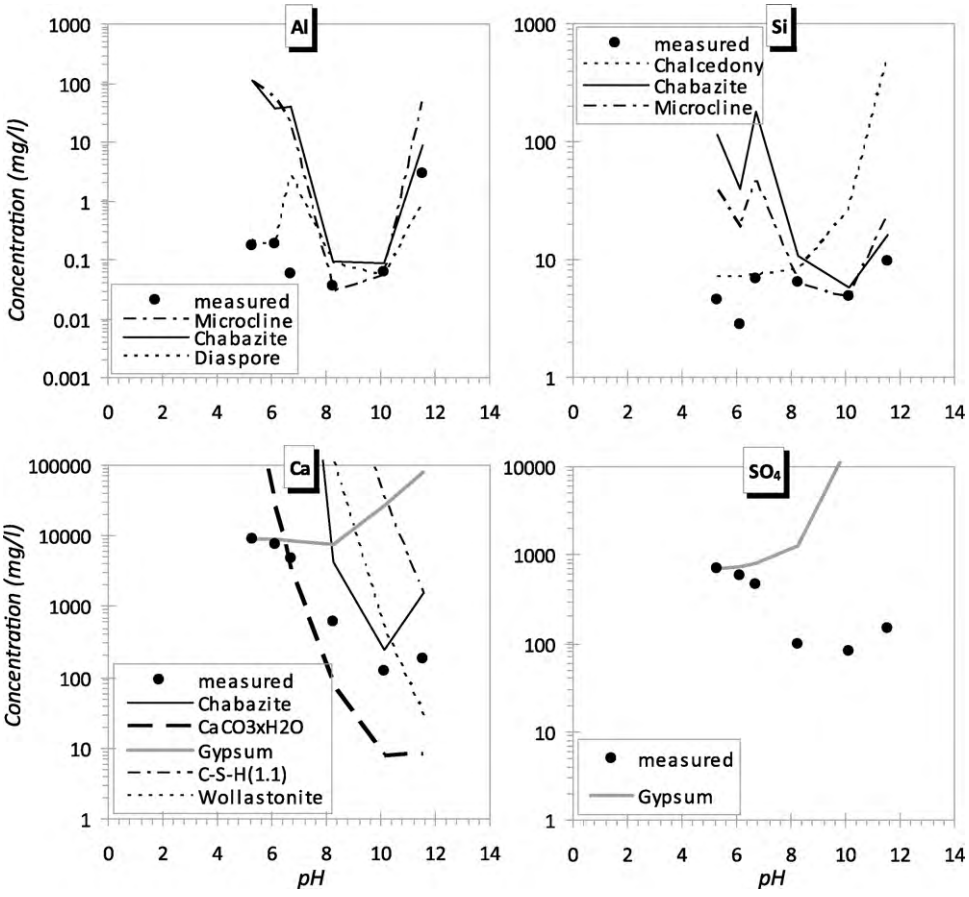

Fig. 10. Experimental data (black dots) and model predictions (continuous lines) for Al, Si, Ca and sulfate leaching from the ACT soil.

was found in the 4-year-old soil. With respect to the microstructure, the ACT soil was characterised by pebble-like structures of clay agglomerations encapsulated in calcium carbonate-rich layers. These structures were a result of the mixing action and the nature of the carbonation reactor utilised in the treatment process.

4.2. Metal leaching

At the time of treatment, the ACT soil had lower contaminant leaching, compared to the freshly treated S/S soils. However, maturation of the S/S soil reduced the metal leaching to levels comparable with the ACT soil, except for Cu. Although in the long term the leaching levels for the metals investigated were comparable for the S/S and the ACT soils at the natural pH of the materials, the analysis of the pH-dependent leaching behaviour showed that the mechanisms governing metal release were significantly different. For the S/S soil, metal release was most likely explained by immobilisation within hydrated alumino-silicate structures whereas for the ACT soil, the precipitation of complex carbonates or sorption onto newly formed minerals may explain the shape of the leaching curves observed. However, further investigation is required to elucidate this matter.

Despite the high concentrations of contaminants in the untreated soil, their availability for leaching was limited. Soil organic matter and clay minerals have strong sorption potential for heavy metals [30], and therefore play an important role in reducing their mobility. The SEM investigation of the untreated soil showed that the contaminants e.g. zinc, were associated with Al-bearing soil minerals, which may have contributed to relatively low leaching even from the untreated soil. The type of interaction between Zn and the clay minerals at the Astra site remains to be established.

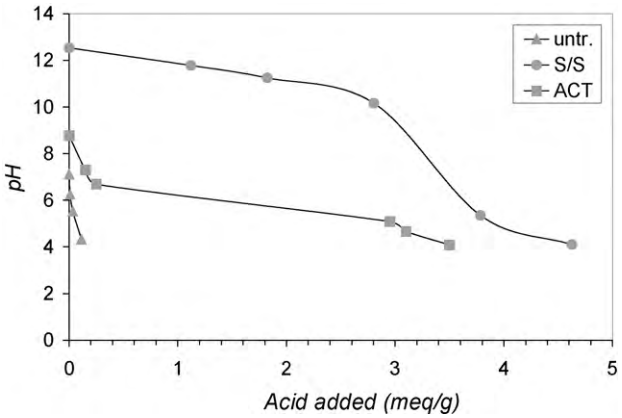

Fig. 11. The ANC curves for the untreated, S/S and ACT soil.

4.3. ANC

The durability of a stabilised soil is not entirely represented by resistance to change in pH; nevertheless the acid neutralisation capacity is a key property of the material; therefore ANC is an important measure of a treated soil potential performance indicator. The results have shown that in terms of the ANC, the two treatments were also distinct and this was mainly due to the binder employed. The untreated soil had a negligible ANC, as shown in Fig. 11. The main buffering occurred below pH 7, in the ACT soil, which was due to carbonate minerals [11], which is in good agreement with the SEM and XRD observations. In contrast with the

ACT, the S/S soil displayed the strongest buffering capacity at high pH ($ANC_{9.0}$). The contributing phases within the pH interval 12–10 are portlandite and variable Ca/Si ratio C–S–H, but also ettringite [39,40].

As shown by the SEM examination and the geochemical modeling, the ACT soil was characterised by carbonates, whereas the S/S soil was dominated by hydrated phases, resulting in an overall $ANC_{4.0}$, lower for the ACT soil than that of the S/S soil. In the literature there are conflicting views on the effect of carbonation on the acid resistance; some authors have reported increase of ANC with accelerated carbonation [9,12] and others a decrease [11,41]. However, Chen et al. [41] observed that dissolution processes in cement stabilised systems, which were carbonated, took place at relatively slower rates compared to the non-carbonated counterparts and therefore may still offer good acid resistance over time.

5. Conclusions

The S/S soil is metastable due to the mineralogical changes observed. Over the 4 years in service, secondary minerals such as ettringite, gypsum and calcium carbonate polymorphs formed. However there is no evidence of disruption in the granular S/S soil.

Carbonation was the most widespread phenomenon occurring in the S/S soil, which resulted in densification of the matrix, by precipitation of calcium carbonate in voids. The findings from geochemical modeling indicated that carbonation was not associated with heavy metal or major elements leaching. The heavy metal leaching was appreciably lower than the predicted values from the oxide, hydroxide and silicates solubility; therefore the metals are likely to be incorporated in the cement hydration phases.

The ACT soil minerals and the 'pebble-like' structure persisted with time, remaining largely unchanged over the 4-year monitoring period. Calcite and aragonite were formed early after the treatment, but only calcite was observed after 4 years.

With regard to the metal immobilisation, the ACT treated soil showed better performance over the S/S soil. Both treatments displayed a significantly improved metal retention compared to the untreated soil. The mechanism of metal immobilisation for the ACT soil was different from that of the S/S soil, with accelerated carbonation being responsible for the formation of pure metal carbonates, especially in the case of Zn. For the other metals investigated, precipitation of complex carbonate phases or sorption onto the surface of neo-formation minerals may explain the actual mechanisms of metal immobilisation within the carbonated matrix.

The results from the experimental programme indicated that the acid resistance of the two treated soils was greatly improved compared to the untreated soils. The increasing order was untreated < ACT < S/S. The buffering capacity of the S/S soil was determined by portlandite, C–S–H, ettringite and calcium carbonate, whereas the ACT was totally reliant on the buffering capacity of the carbonate phases present.

Acknowledgements

The authors would like to thank SITA Environmental UK for their financial support.

References

[1] Environment Agency, Available on line at: http://www.environment-agency.gov.uk/research/library/data/34403.aspx, 2009.
[2] C.N. Mulligan, R.N. Yong, B.F. Gibbs, Remediation technologies for metal-contaminated soils and groundwater: an evaluation, Eng. Geol. 60 (1–4) (2001) 193–207.
[3] G. Dermont, M. Bergeron, G. Mercier, M. Richer-Laflèche, Metal-contaminated soils: remediation practices and treatment technologies, Pract. Period. Hazard. Toxic Radioact. Waste Manage. 12 (3) (2008) 188–209.
[4] J. Conner, Chemical Fixation and Solidification of Hazardous Wastes, Van Nostrand Reinhold, New York, 1990.
[5] L.H. Barnard, D.I. Boardman, C.D.F. Rogers, C.D. Hills, P.J. Carey, K. Canning, C.L. MacLeod, Influence of soil and binder properties on the efficiency of accelerated carbonation, in: A. Al-Tabbaa, J. Stegemann (Eds.), Stabilisation/Solidification Treatment and Remediation, Taylor and Francis Group, London, 2005, pp. 365–387.
[6] J.R. Fitch, C.R. Cheeseman, Characterisation of environmentally exposed cement-based stabilised/solidified industrial waste, J. Hazard. Mater. 101 (3) (2003) 239–255.
[7] I. Klich, L.P. Wilding, L.R. Drees, E.R. Landa, Importance of microscopy in durability studies of solidified and stabilized contaminated soils, Soil Sci. Soc. Am. J. 63 (1999) 1274–1283.
[8] X. Li, M. Fernandez Bertos, C.D. Hills, P.J. Carey, S. Simon, Accelerated carbonation of municipal solid waste incineration fly ashes, Waste Manage. 27 (2007) 1200–1206.
[9] A. Polettini, R. Pomi, The leaching behavior of incinerator bottom ash as affected by accelerated ageing, J. Hazard. Mater. B113 (2004) 209–215.
[10] L.C. Lange, C.D. Hills, A.B. Poole, The effect of accelerated carbonation on the properties of cement-solidified waste forms, Waste Manage. 16 (8) (1996) 757–763.
[11] R.E.H Sweeney, Accelerated carbonation of solidified hazardous wastes, PhD Thesis, Imperial College, London, 2001.
[12] M. Fernández Bertos, S.J.R. Simons, C.D. Hills, P.J. Carey, A review of accelerated carbonation technology in the treatment of cement-based materials and sequestration of CO_2, J. Hazard. Mater. 112 (2004) 193–205.
[13] D. Barr, R.P. Bardos, C.P. Nathanail, Non-biological methods for assessment and remediation of contaminated land—case studies, CIRIA, 2003.
[14] CLAIRE. Remediation Trial at the Avenue Coking Works Using Stabilisation/Solidification and Accelerated Carbonation Technology. Case Study Bulletin CB5. 2006.
[15] A.S.R. Perera, A. Al-Tabbaa, J.M. Reid, J.A. Stegemann, Part IV: Testing and performance criteria. In: A. Al-Tabbaa, J. Stegemann (Eds), Stabilisation/Solidification Treatment and Remediation Advances in S/S for Waste and Contaminated Land, pp. 415–435.
[16] Blue Circle, Accelerated Carbonation for the Remediation of Contaminated Land, Phase 2—Evaluation of Binder Types, Unpublished Report, University of Greenwich (2002).
[17] D.M. Moore, R.C. Reynolds Jr., X-ray Diffraction and the Identification and Analysis of Clay Minerals, second ed., Oxford University Press, Oxford, 1997.
[18] United States Environmental Protection Agency, Method 1311. Toxicity Characteristics Leaching Procedure. Test Methods for Evaluating Solid Wastes Physical/Chemical Methods. USEPA Report Number: SW-846. 1980.
[19] DIN-NORMEN DIN 38414 S4. Determination of leachability by water (S4). German standard methods for examination of water, wastewater and sludge. Sludge and Sediments (group S). 1984.
[20] prCEN/TS 15364 Characterization of waste—leaching behaviour tests—acid and base neutralization capacity test. 2005.
[21] T. Astrup, J. Dijkstra, R.N.J. Comans, H.A. van der Sloot, T.H. Christensen, Geochemical modelling of leaching from MSWI air-pollution-control residues, Environ. Sci. Technol. 40 (2006) 3551–3557.
[22] B. Lothenbach, F. Winnefeld, Thermodynamic modeling of the hydration of Portland cement, Cement Concrete Res. 36 (2006) 209–226.
[23] P. Blanc, A. Lassin, C. Nowak, A. Burnol, P. Piantone, L. Chateau, THERMODDEM: a thermodynamic database for waste materials. Available on-line at http://thermoddem.brgm.fr/fichiers/Phreeqc_thermoddem_lvl1_no-org.txt. 2007.
[24] J.J. Dijkstra, H.A. van der Sloot, R.N.J. Comans, Process identification and model development of contaminant transport in MSWI bottom ash, Waste Manage. 22 (2002) 531–541.
[25] J. Hyks, T. Astrup, T.H. Christensen, Long-term leaching from MSWI air pollution control residues: leaching characterization and modelling, J. Hazard. Mater. 162 (2009) 80–91.
[26] C.D. Hills, Personal Communication, University of Greenwich, 2009.
[27] G. Taylor, The occurrence of monohydrocalcite in two small lakes in the South-East of South Australia, Am. Mineral. 60 (1975) 690–697.
[28] H. Elfil, H. Roques, Role of hydrate phases of calcium carbonate on the scaling phenomenon, Desalination 137 (2001) 177–186.
[29] A.C. Garrabrants, D.S. Kosson, Leaching processes and evaluation tests for inorganic constituent release from cement-based matrices, in: R.D. Spence, C. Shi (Eds.), Stabilisation/Solidification of Hazardous, Radioactive and Mixed Wastes, CRC Press, Boca Raton, 2005, pp. 177–199.
[30] Environment Agency, Guidance on the use of Stabilisation/Solidification for the Treatment of Contaminated Soil Science Report: SC980003/SR1, 2004.
[31] D.A.St. John, A.W. Poole, I. Sims, Concrete Petrography. A Handbook of Investigative Techniques, Elsevier/Butterworth-Heinemann, Oxford, 1998.
[32] M. Collepardi, A state-of-the-art review on delayed ettringite attack on concrete, Cem. Concr. Compos. 25 (2003) 401–407.
[33] O.R. Batic, C.A. Milanesi, P.J. Maiza, S.A. Marfil, Secondary ettringite formation in concrete subjected to different curing conditions, Cement Concrete Res. 30 (2000) 1407–1412.
[34] H.F.W. Taylor, C. Famy, K.L. Scrivener, Delayed ettringite formation, Cement Concrete Res. 31 (2001) 683–693.

[35] S. Diamond, Delayed ettringite formation—processes and problems, Cement Concrete Compos. 18 (1996) 205–215.
[36] W.A. Klemm, Etringite and Oxyanion-Substituted Ettringite—their characterisation and applications in the fixation of heavy metals: a synthesis of the literature, Portland Cement Association, Skokie, IL, USA, 1998.
[37] W.G. Hime, B. Mather, "Sulfate attack," or is it? Cement Concrete Res. 29 (1999) 789–791.
[38] C.D. Lawrence, The constitution and specification of Portland Cements, in: P.C. Hewlett (Ed.), Lea's Chemistry of Cement and Concrete Fourth Edition, Elsevier/Butterworth-Heinemann, Oxford, 1988, pp. 131–188.
[39] C. Giampaolo, S. Lo Mastro, A. Polettini, R. Pomi, P. Sirini, Acid neutralisation capacity and hydration behaviour of incineration bottom ash–Portland cement mixtures, Cement Concrete Res. 32 (2002) 769–775.
[40] J.A. Stegemann, C. Shi, R.J. Caldwell, Acid resistance of different monolithic binders and solidified wastes, in: J.J.J.M. Goumans, G.J. Senden, H.A. van der Sloot (Eds.), Studies in Environmental Science 71. Waste Materials in Construction: Putting Theory into Practice, Elsevier, 1997, pp. 551–562.
[41] Q. Chen, L. Zhang, Y. Ke, C.D. Hills, Y. Kang, Influence of carbonation on the acid neutralization capacity of cements and cement-solidified/stabilized electroplating sludge, Chemosphere 74 (2009) 758–764.